Supplementary Material

Functional transcriptional regulatory sequence (TRS) RNA binding and helix destabilizing determinants of the murine hepatitis virus (MHV) nucleocapsid (N) protein

Sarah C. Keane, Pinghua Liu, Julian L. Leibowitz and David P. Giedroc

This file contains Supplementary Methods Table S1, Figures S1-S11.

Supplementary Methods

Nonlinear Least Squares Fitting Models.
Model 1. Equilibrium titration of NTD into F-TRS RNA:
NTD + F-TRS ←→ NTD-F-TRS K_{obs}

Model 2. Equilibrium titration of NTD into a duplex TRS-cTRS Cy3/Cy5 pair:
TRS + cTRS ←→ dsTRS (annealing) K_1 (fixed)
NTD + TRS ←→ NTD-TRS K_2 (fixed)
NTD + cTRS ←→ NTD-cTRS K_3 (fixed)
NTD + dsTRS ←→ NTD-dsTRS K_4

Table S1. Paramagnetic broadening that results from incorporation of a nitroxide radical at position 2 or 9 in TRS RNA.[a]

Residue	I_{para}/I_{dia} (MTSL-U2, 5')	I_{para}/I_{dia} (MTSL-U9, 3')	Broadening location [b]
66	0.93	0.88	
68	0.65	0.82	
69	0.75	0.79	
70	0.91	0.55	U9
72	0.97	0.81	U9
76	1.11	0.79	U9
79	0.99	0.98	
80	0.91	1.03	
82	1.26	1.48	
83	1.01	1.11	
84	1.05	0.84	U9
85	0.93	1.05	
86	1.01	1.06	
87	0.96	1.06	

88	1.06	1.07	
89	1.16	1.11	
91	1.00	1.03	
92	0.90	1.08	
95	0.76	0.93	U2
98	0.99	1.10	
99	1.03	1.11	
100	1.06	1.07	
101	1.07	1.12	
102	1.05	1.08	
103	0.93	1.16	
104	1.02	1.07	
106	0.89	0.98	
109	0.74	0.88	
116	0.87	0.73	
117	0.86	0.98	
118	0.95	0.94	
119	0.69	0.96	U2
120	0.68	0.91	U2
122	0.76	0.44	U9
125	0.99	0.84	U9
126	0.78	0.43	U9
128	0.91	1.05	
129	0.94	1.07	
130	0.74	0.92	U2
131	0.75	1.03	U2
132	0.98	1.01	
133	0.93	1.08	
136	0.66	0.88	U2
137	0.60	0.88	U2
138	0.69	0.99	U2
139	1.11	1.06	
140	0.65	1.05	U2
141	0.95	1.04	
143	1.01	1.10	
144	0.71	1.02	U2
145	0.93	1.06	U2
146	0.82	0.99	U2
147	0.86	0.98	U2
148	0.95	1.13	
149	1.06	1.13	
150	1.05	1.04	
151	1.05	1.09	
152	1.02	1.08	

153	1.00	1.05	
154	0.94	1.06	
155	0.99	1.04	
156	1.05	1.06	
157	0.95	1.13	
158	0.99	1.05	
160	1.00	1.08	
163	0.92	1.02	
164	1.05	1.09	
165	0.31	0.46	U2
166	0.85	1.08	U2
167	0.99	1.11	
168	0.94	1.10	
170	0.77	0.82	
171	0.88	1.00	
172	0.80	1.00	
174	0.97	1.05	
175	0.88	0.98	
177	1.16	0.89	U9
178	1.05	0.91	
183	0.92	0.97	
184	1.06	1.04	
185	0.95	0.82	
188	0.51	0.57	
189	0.82	0.58	U9

[a] Only residues that make up the structural core (aa 64-194) of the MHV NTD were included in this analysis. Residues with overlapped amide resonances or signal:noise ratios below 10 were excluded from this analysis.

[b]Amide resonances defined as differentially broadened by U2-SL of U9-SL are those in which I_{para}/I_{dia} for one RNA is ≥15% different from that of the other RNA. Amide resonances defined as differentially broadened by U2-SL (denoted U2, near 5'-end of TRS RNA) are painted red on Fig. 3C, main text. Amide resonances defined as differentially broadened by U9-SL (denoted U9, near 3'-end of TRS RNA) are painted red on Fig. 3D, main text.

The error of the measurement was determined using the equation $\sigma = ((\sigma_{dia}/I_{dia})^2+(\sigma_{para}/I_{para})^2)^{1/2}/(I_{dia}/I_{para})$ where σ_{dia} and σ_{para} are the signal to noise value of a resonance and I_{dia} and I_{para} are the data height of a resonance in the diamagnetic and paramagnetic spectra respectively. All errors were $\leq 2.0 \times 10^{-4}$.

Fig. S1. *A*. Multiple sequence alignment of CoV NTDs using ClustalW. Betacoronaviruses (group a): MHV-A59 (NC_001846), BCoV (NC_003045), HCoV-OC43 (NC_005147), HKU1 (NC_006577). Betacoronaviruses (group b) CoV: SARS (NC_004718). Alphacoronaviruses: HCoV-NL63 (NC_005831), HCoV-229E (NC_002645), TGEV (DQ811789.2). Gammacoronavirus: IBV (NC_001451). *B*. Phylogenetic analysis of CoV N proteins.

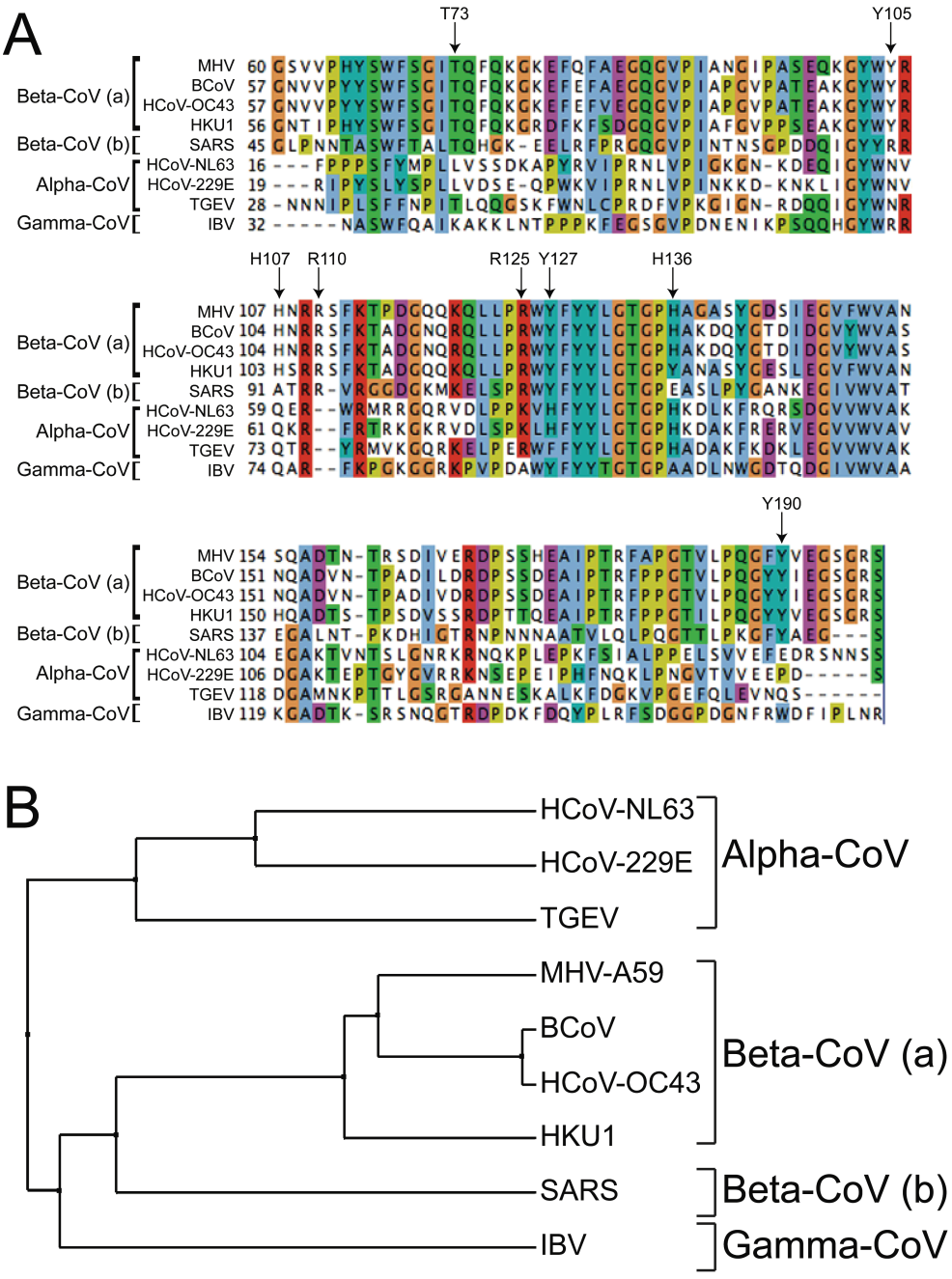

Fig. S2. $^{1}H,^{15}N$ HSQC overlay of N197 (≈200 µM, blue) and N1-230 (≈200 µM, red).

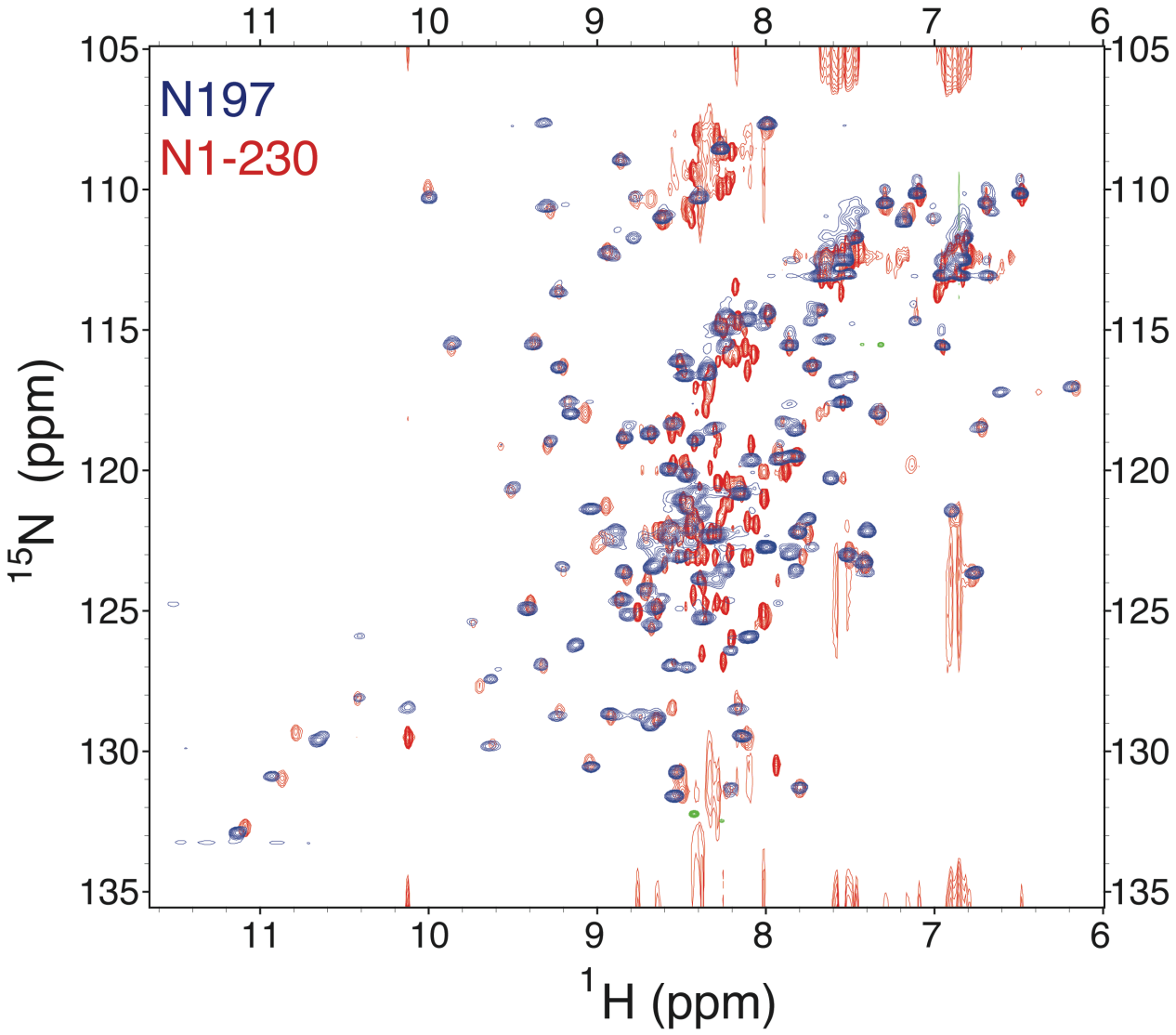

Fig. S3. N219 R125A F-TRS binding isotherm that results from an overnight incubation of protein and RNA in the dark at 25 °C. The continuous line represents a nonlinear least squares fit to 1:1 binding model with the initial anisotropy (r_o) fixed to the measured value for free F-TRS RNA (r_o=0.8), with the final value ($r_{complex}$) and K_{obs} optimized during the fit to 0.22 and 3.7 x 10^6 M^{-1}, respectively.

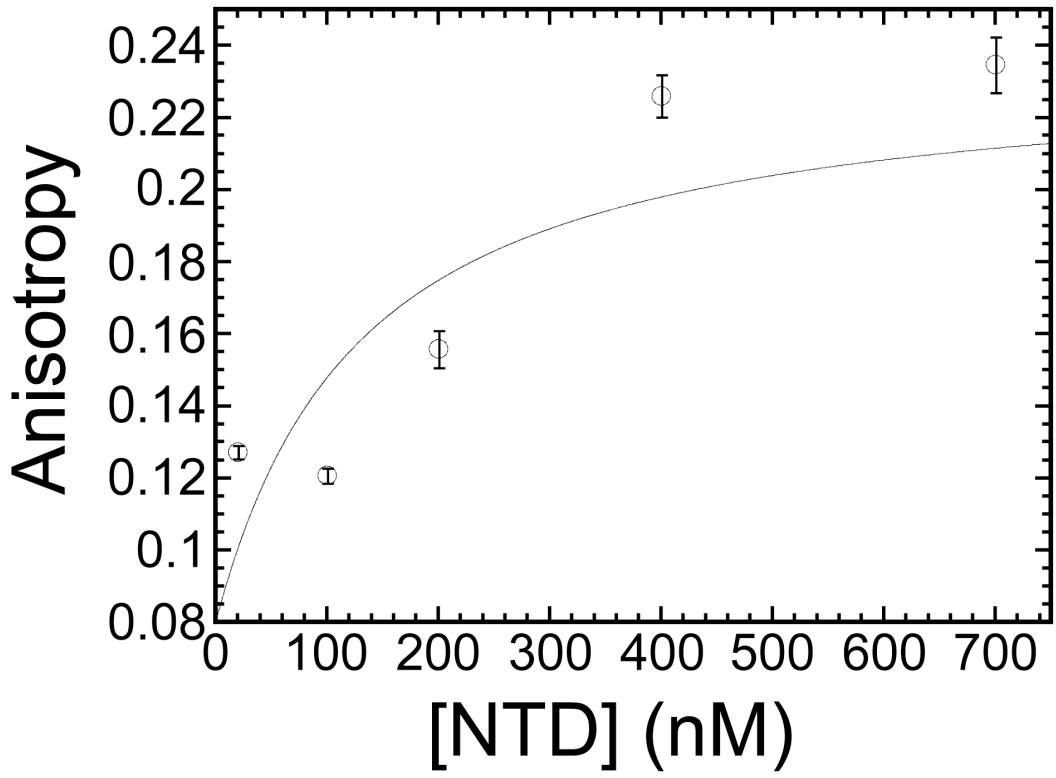

Fig. S4. Chemical shift perturbation map of single point mutations in a N219 construct. *A*, R125A N219 *B*, Y190A N219. Secondary structure is shown at the top of each plot. Pound symbols represent proline residues for which there is no HSQC cross-peak.

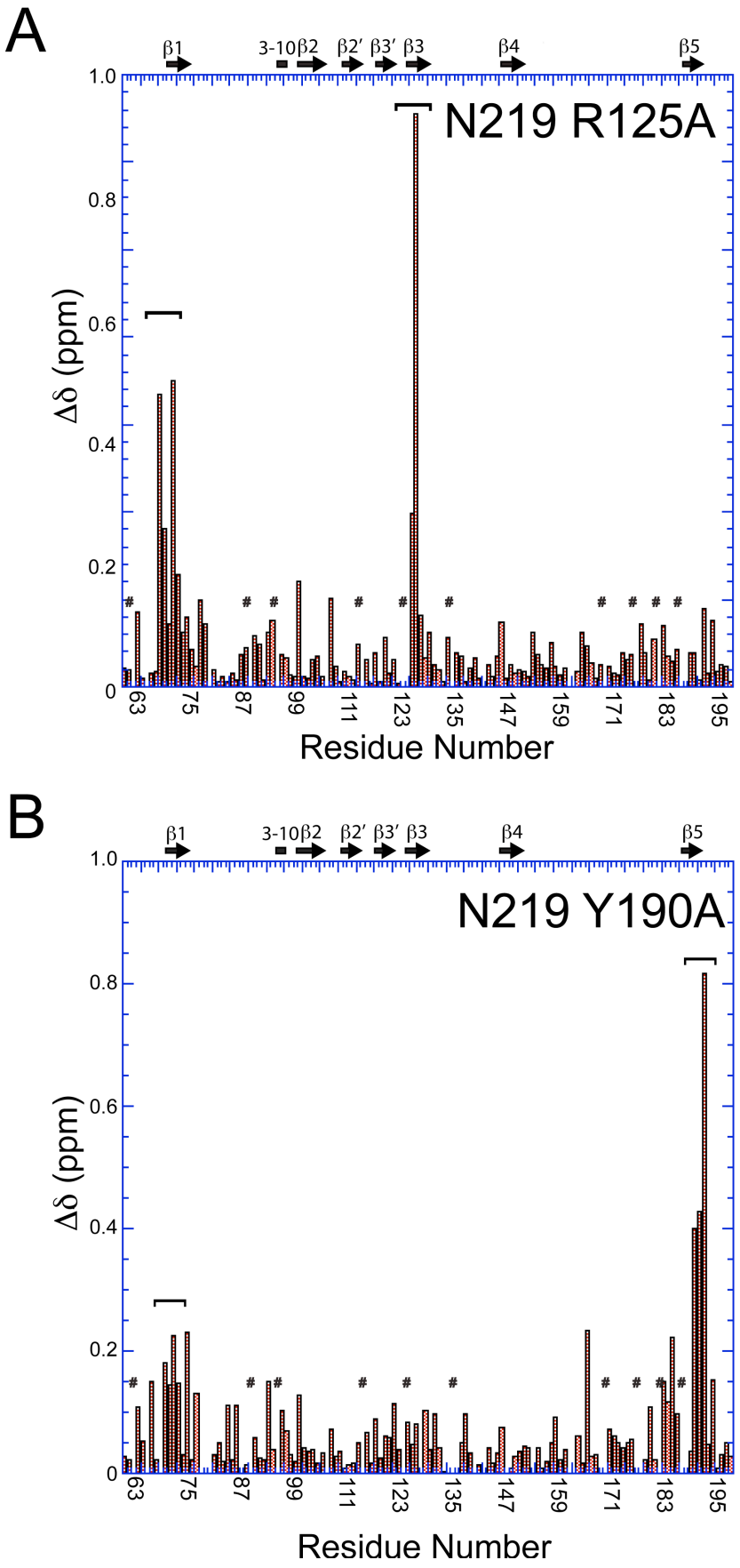

Fig. S5. Selected region of ^{1}H,^{15}N HSQC spectra of free N197 (*blue*) with N197-TRS complex (*magenta*, *green*) at *A*, 600 MHz and *B*, 800 MHz. Amide group resonance assignments are 95% complete (seven non-Pro residues are unassigned), with five unassigned (and broadened) resonances indicative of substantial dynamics even in the free protein (1). Residues that lie in the protein-RNA interface are labeled in bold and italics. At 600 MHz, RNA binding induces both line broadening and a change in chemical shift. In contrast, at 800 MHz formation of the NTD-TRS complex induces significant line broadening of residues that are at or near the protein-RNA interface. These differential field-dependent effects and an intermediate exchange regime are fully consistent with $K_{obs} \approx 10^{7}$ M^{-1} under these conditions (Table 1, main text).

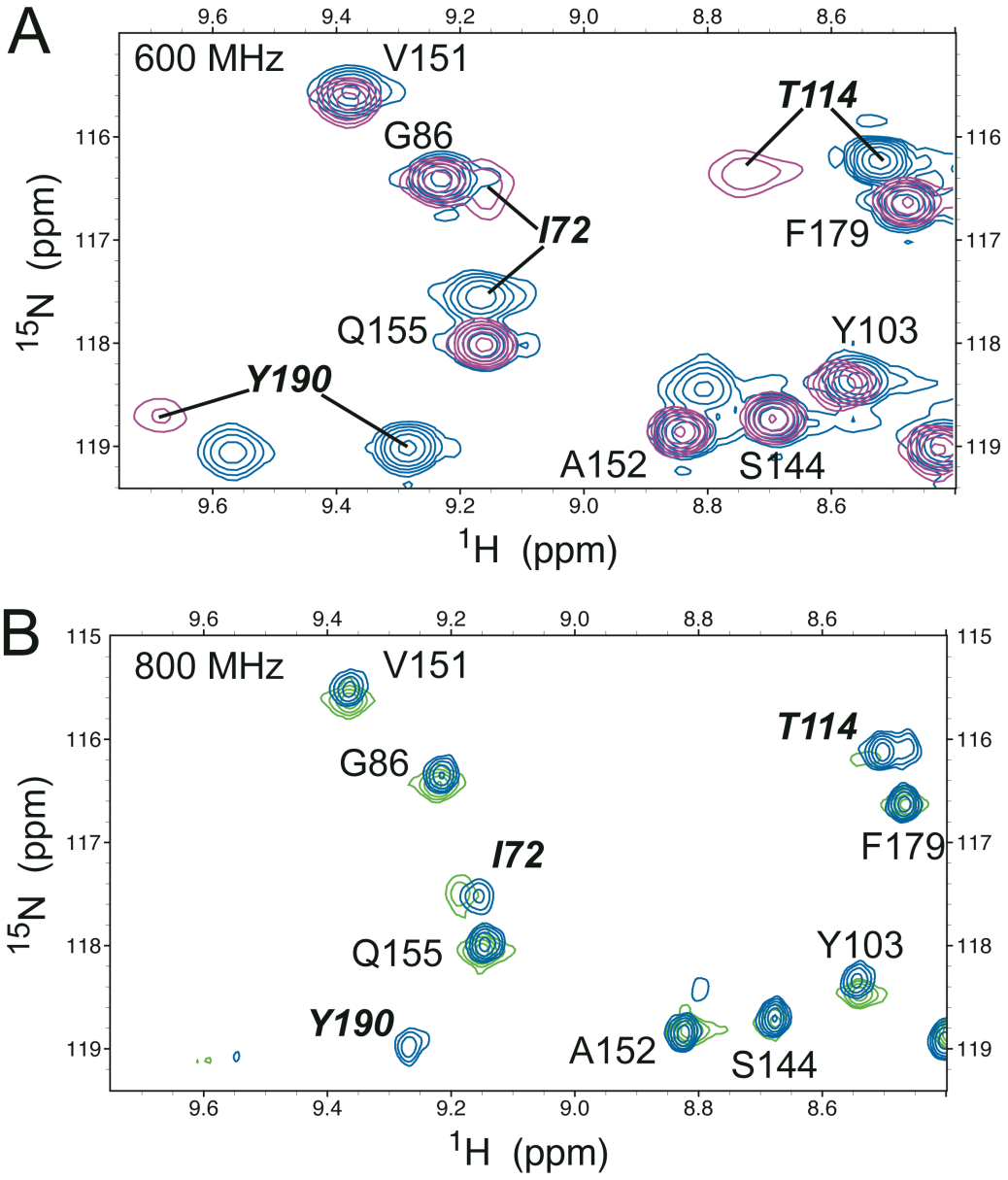

Fig. S6. Structures of *A*. the 4-thiouridine base, *B*. (1-Oxyl-2,2,5,5-tetramethyl-Δ3-pyrroline-3-methyl) Methanethiosulfonate (MTSL) spin label reagent, and *C*. the spin-labeled 4-thiouridine base.

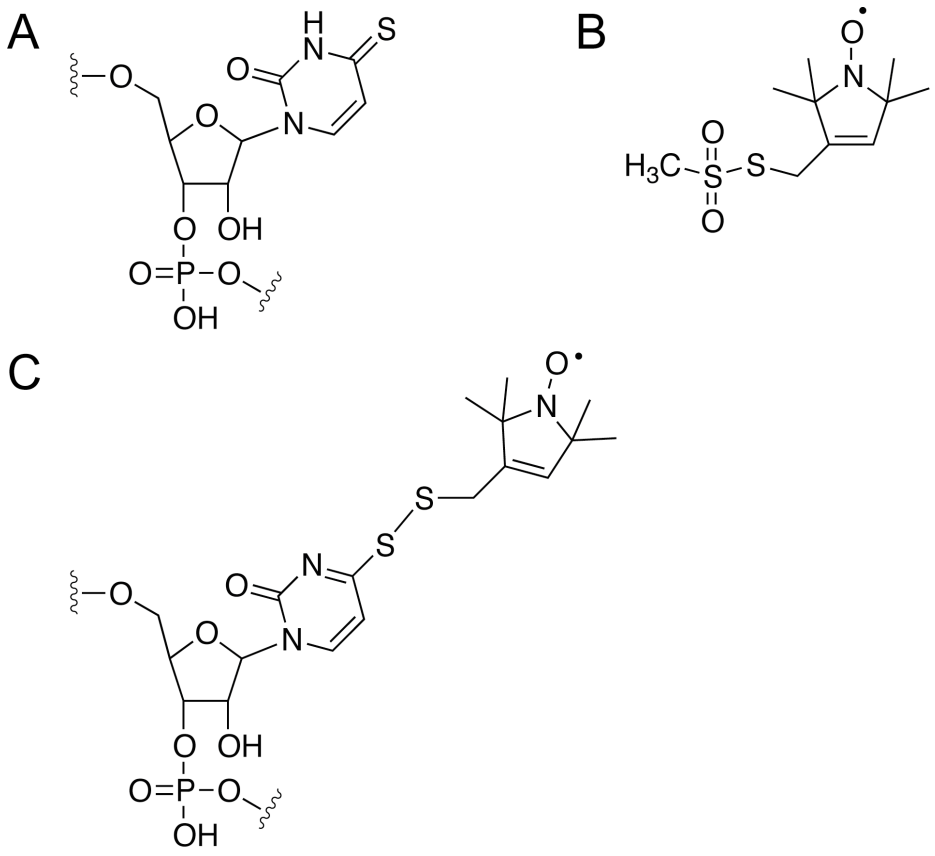

Fig. S7. Kinetics of TRS-cTRS helix destabilization by various NTD proteins. N197 (green solid circles, ●), N1-230 (blue solid circles, ●), N60-230 (cyan solid up triangles, ▲), N219 Y105A (red solid squares, ■), N219 H107A (yellow solid up triangles, ▲), and N219 H136A (orange solid diamonds, ◆). The solution conditions are described in Fig. 4 (main text), with 50 nM RNA duplex and 5 μM total NTD protein.

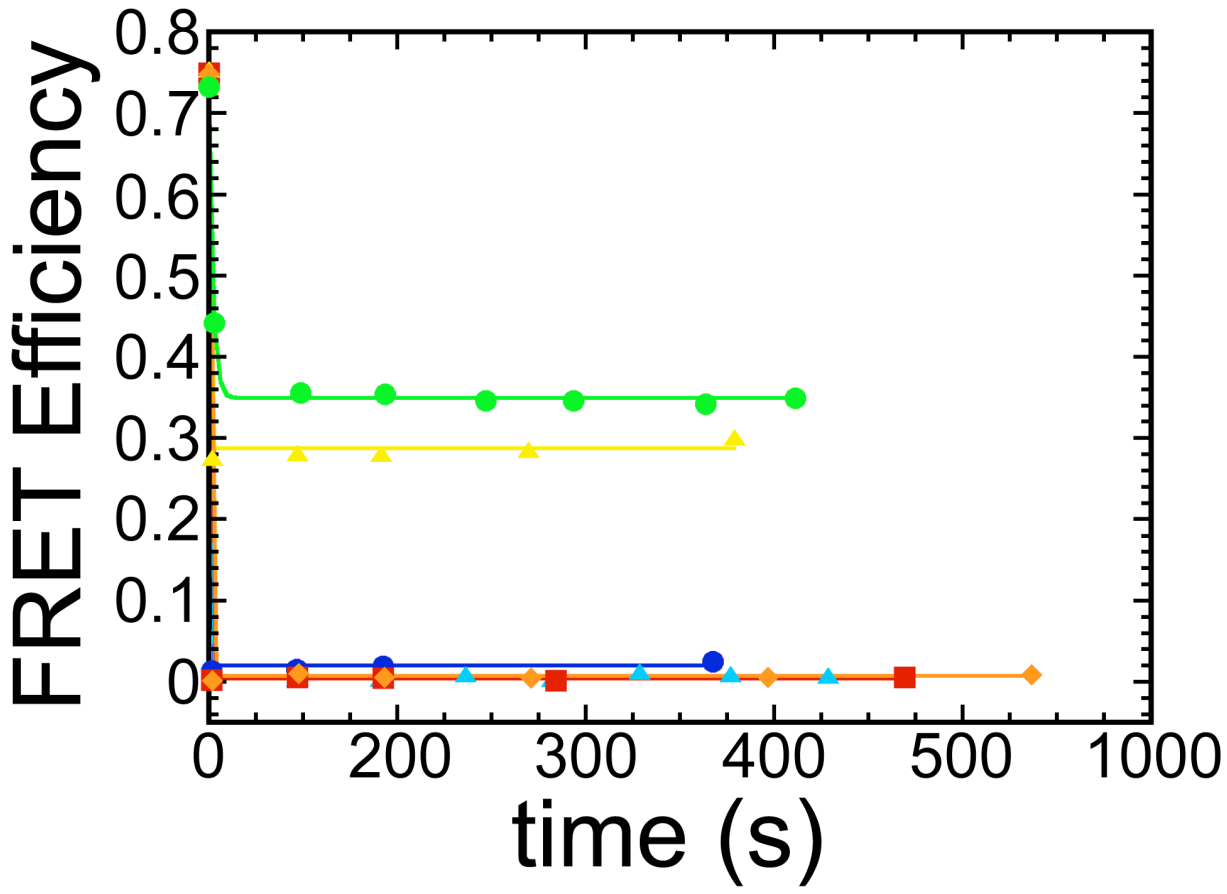

Fig. S8. MHV NTD binds with MHV TRS (blue closed circles ●) SARS-CoV TRS (orange closed squares ■) and IBV TRS (green closed diamonds ◆). See Table 3, main text for fitted parameters.

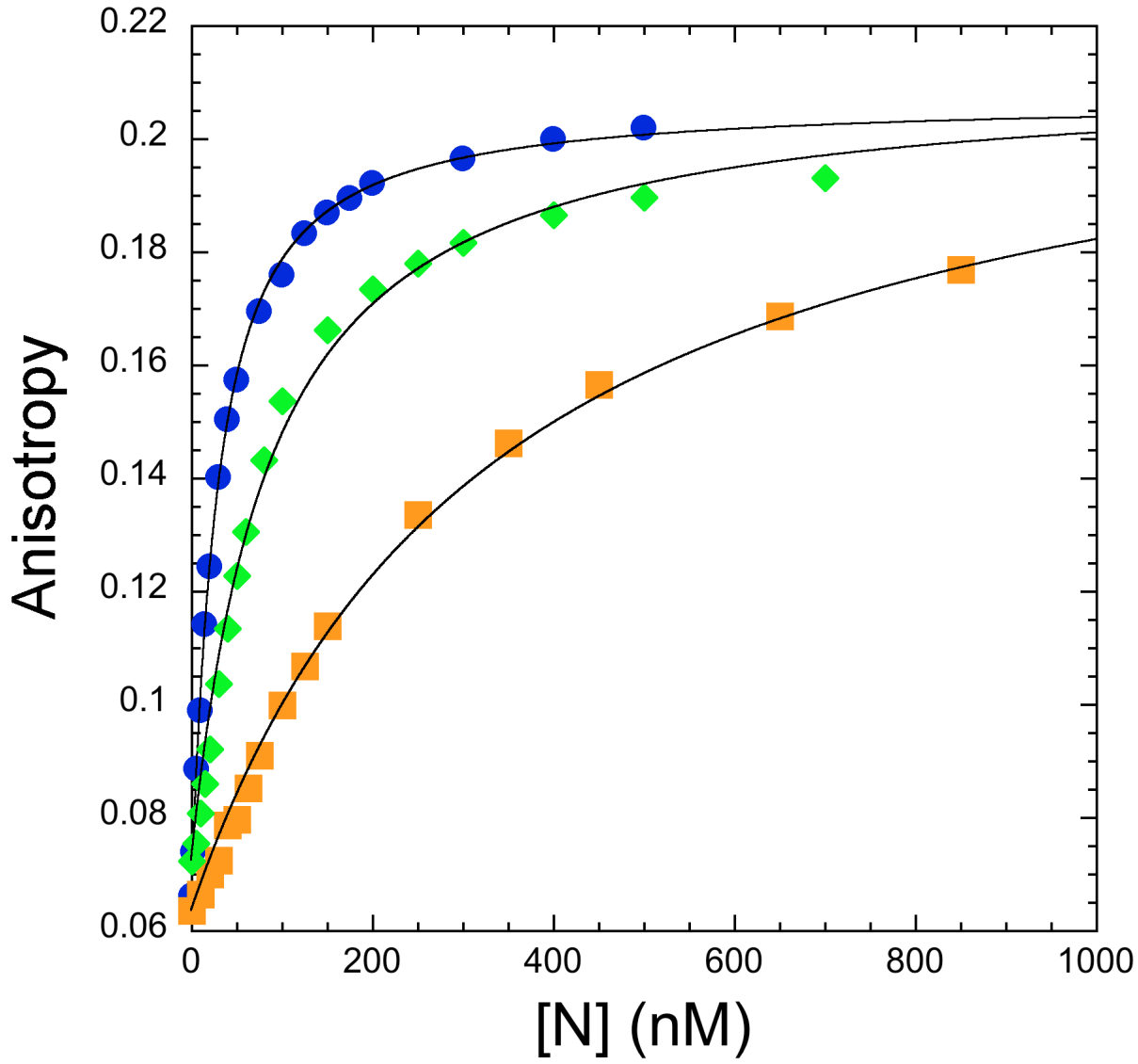

Fig. S9. Sequence alignment of RNAs used in this work. MHV NTD binding affinities are shown at *right* (see Table 3, main text). A consensus sequence is present and conserved for all high affinity RNAs ($K_a \geq 10^7$ M^{-1}). Substitutions within this consensus sequence result in decreased RNA binding affinity.

RNA	sequence (5′-3′)	Affinity (x10^7 M^{-1})
MHV TRS	AAUCUAACU	4.3
Scrambled	AUCUAGCUAU	1.7
IBV TRS	GAACUUAACA	1.3
SARS TRS	AA**A**C**G**AACUU	0.3
Random10	AU**A**UAGCUAC	0.2
Consensus	AYYUAR(A/C)Y	

Fig. S10. Standard salt-back titration of the IBV NTD-IBV TRS complex. IBV NTD (5 μM, $[P]_{total}$) was added to IBV F-TRS (10 nM, $[R]_{total}$) and competed off with addition of concentrated KCl to the indicated concentration. K_{obs} was calculated for the *i*th concentration of salt from the measured anisotropy at each point, r_i, as follows:

$$K_{obs} = [PR]/[P]\bullet[R]$$
$$\Theta = (r_i - r_0)/(r_{complex} - r_0)$$
$$[PR] = \Theta \bullet [R]_{total}$$
$$[P] = [P]_{total} - [PR]$$
$$[R] = [R]_{total} - [PR]$$

where the initial anisotropy (r_0) and anisotropy of the saturated protein-RNA complex ($r_{complex}$) were fixed at 0.069 and 0.170 (see also Table 3, main text), respectively, and $[P]_{total}$ and $[R]_{total}$ corrected for dilution. Only the linear portion of the salt-back data is shown below.

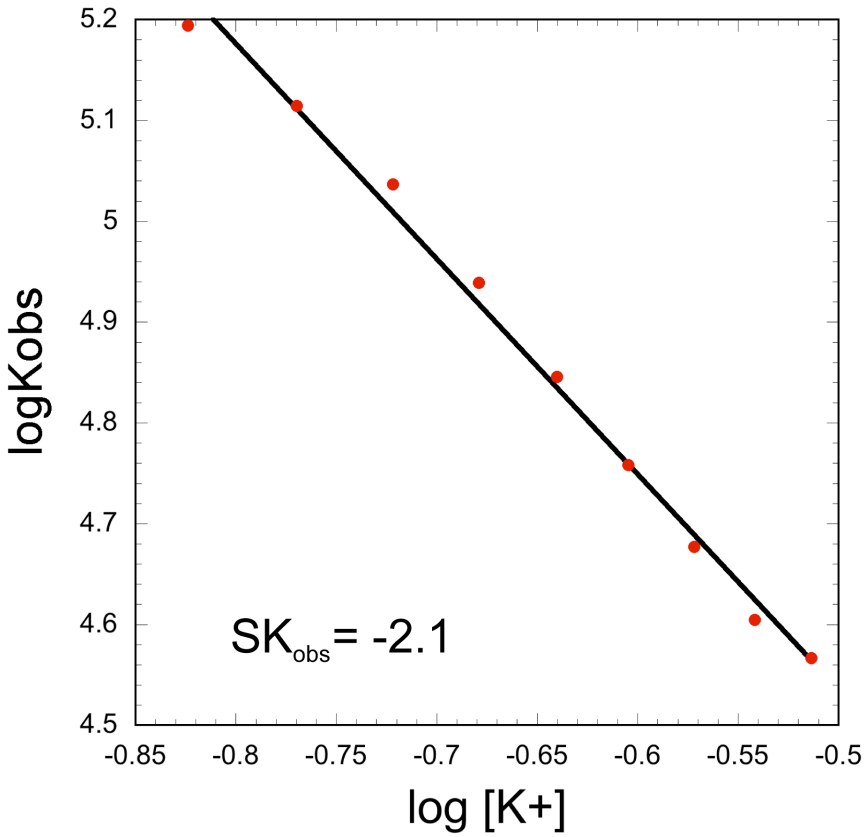

Fig. S11. IBV NTD WT (blue closed circles ●) and R76A (red closed diamonds ◆) bind to IBV TRS with comparable affinities. In contrast, IBV NTD Y94A (cyan closed squares ■) binds to IBV TRS with considerably weaker affinity. See Table 3, main text for fitted parameters.

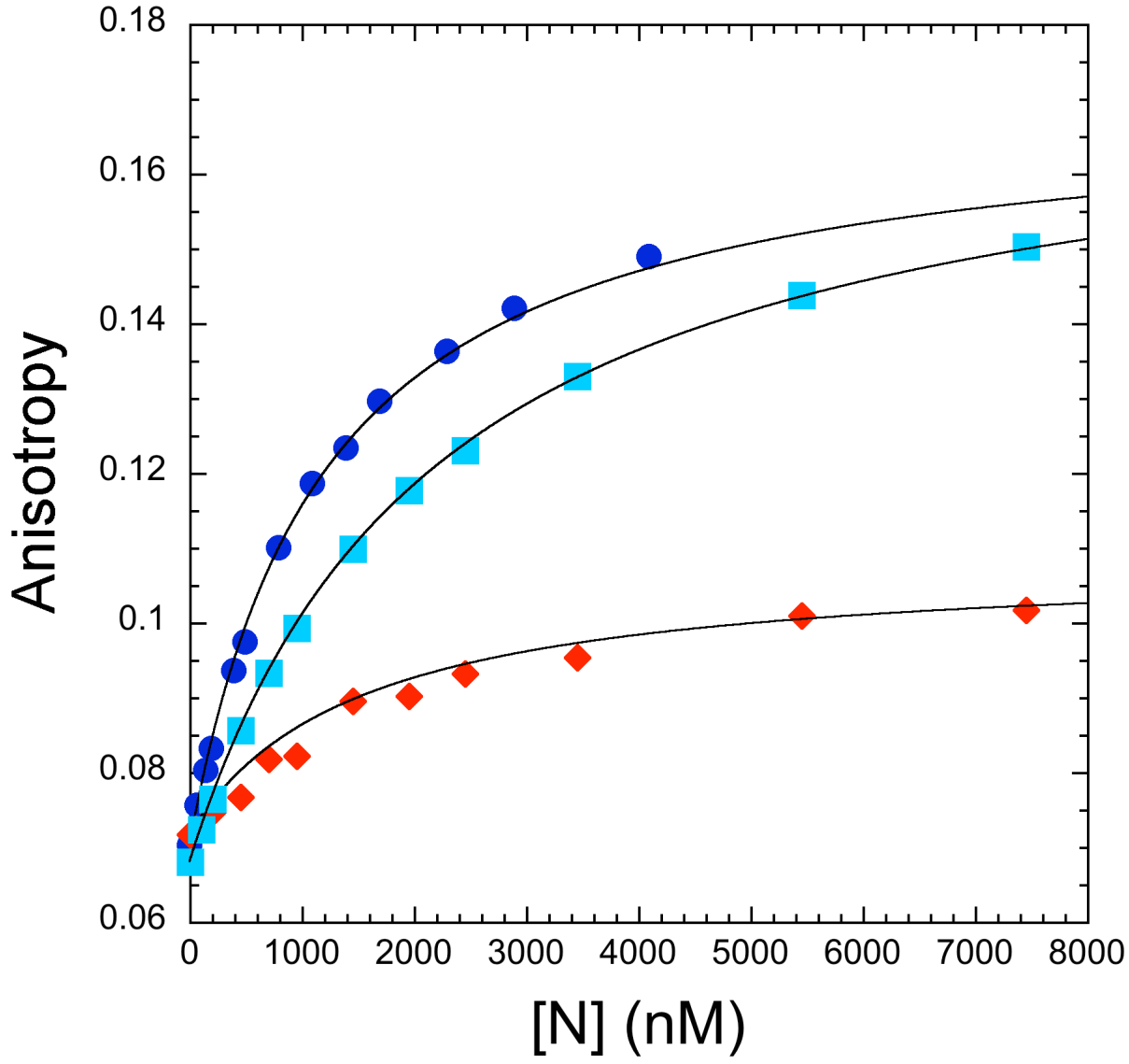

REFERENCES

1. Clarkson, M. W., Lei, M., Eisenmesser, E. Z., Labeikovsky, W., Redfield, A., and Kern, D. (2009) *J. Biomol. NMR* **45**, 217-225